Improved drug delivery to brain metastases by peptide-mediated permeabilization of the blood-brain barrier

List of authors

Synnøve Nymark Aasen[1,2], Heidi Espedal[2,3], Christopher Florian Holte[2], Olivier Keunen[4], Tine Veronika Karlsen[5], Olav Tenstad[5], Zaynah Maherally[6], Hrvoje Miletic[2,7], Tuyen Hoang[2], Anne Vaag Eikeland[8], Habib Baghirov[9], Dag Erlend Olberg[10,11], Geoffrey John Pilkington[6], Gobinda Sarkar[12], Robert B. Jenkins[12], Terje Sundstrøm[2,13,14], Rolf Bjerkvig[2,4,*] and Frits Thorsen[2,3,*]

Affiliations

[1] Department of Oncology and Medical Physics, Haukeland University Hospital, Bergen, Norway.

[2] Kristian Gerhard Jebsen Brain Tumour Research Centre, Department of Biomedicine, University of Bergen, Bergen, Norway.

[3] Molecular Imaging Center, Department of Biomedicine, University of Bergen, Bergen, Norway.

[4] Department of Oncology, Luxembourg Institute of Health, Luxembourg, Luxembourg.

[5] Department of Biomedicine, University of Bergen, Bergen, Norway.

[6] Brain Tumour Research Centre, Institute of Biomedical and Biomolecular Sciences, University of Portsmouth, Portsmouth, PO1 2DT, UK.

[7] Department of Pathology, Haukeland University Hospital, Bergen, Norway.

[8] Department of Radiology, Haukeland University Hospital, Bergen, Norway.

[9] Department of Physics, Norwegian University of Science and Technology, Trondheim, Norway.

[10] Department of Pharmaceutical Chemistry, University of Oslo, Oslo, Norway.

[11] Norwegian Cyclotron Center, Oslo University Hospital, Oslo, Norway.

[12] Division of Experimental Pathology, Mayo Clinic, Rochester MN, USA.

[13] Department of Neurosurgery, Haukeland University Hospital, Bergen, Norway.

[14] Department of Clinical Medicine, University of Bergen, Bergen, Norway.

* Equal contributions

Running title: Peptide-mediated drug delivery to brain metastases

Correspondence to: Frits Thorsen, Department of Biomedicine, University of Bergen, Jonas Lies vei 91, N-5009, BERGEN, Norway. Phone: +47 95749681. E-mail: Frits.Thorsen@uib.no

Conflict of interest statement: The authors declare no potential conflict of interest.

Keywords: Brain metastases, K16ApoE, blood-brain barrier (BBB), drug delivery, targeted therapy

Abstract

Melanoma patients have a high risk of developing brain metastasis, which is associated with a dismal prognosis. During early stages of metastasis development, the blood-brain barrier (BBB) is likely intact, which inhibits sufficient drug delivery into the metastatic lesions. We investigated the ability of the peptide, K16ApoE, to permeabilize the BBB for improved treatment with targeted therapies preclinically. DCE-MRI was carried out on NOD/SCID mice to study the therapeutic window of peptide-mediated BBB permeabilization. Further, both *in vivo* and *in vitro* assays were used to determine K16ApoE toxicity and to obtain mechanistic insight into its action on the BBB. The therapeutic impact of K16ApoE on metastases was evaluated combined with the mitogen-activated protein kinase pathway inhibitor dabrafenib, targeting BRAF mutated melanoma cells, which is otherwise known not to cross the intact BBB. Our results from the DCE-MRI experiments showed effective K16ApoE-mediated BBB permeabilization lasting for up to one hour. Mechanistic studies showed a dose-dependent effect of K16ApoE caused by induction of endocytosis. At concentrations above IC_{50}, the peptide additionally showed nonspecific disturbances on plasma membranes. Combined treatment with K16ApoE and dabrafenib reduced the brain metastatic burden in mice and increased animal survival, and PET/CT showed that the peptide also facilitated the delivery of compounds with molecular weights as large as 150 kDa into the brain. To conclude, we demonstrate a transient permeabilization of the BBB, caused by K16ApoE, that facilitates enhanced drug delivery into the brain. This improves the efficacy of drugs that otherwise do not cross the intact BBB.

Introduction

Brain metastasis is a frequently reported complication for patients with cutaneous melanoma where the average survival time, if untreated, is 3–5 months. Current treatment strategies involve surgery, systemic therapy, radiotherapy and/or radiosurgery (1). This can to some extent increase the survival time, yet with a divergent treatment efficacy, emphasizing the need for new treatment options.

It is well known that melanomas are molecularly heterogeneous (2) and immunogenic tumors (3), properties that have been exploited for drug development (4). For instance, it has been shown that the serine/threonine kinase protein BRAF is a key molecular driver of metastatic melanoma, which has led to the development of several BRAF inhibitors (BRAFi). Furthermore, immune checkpoint inhibitors such as PD-1/PD-L1 have shown a strong clinical efficacy in clinical trials for melanoma (5-7). However, a recurring issue is that many of these drugs are too large to cross the intact interface between circulating blood and the brain parenchyma, i.e. the blood-brain barrier (BBB) (8,9). The BBB consists of vascular endothelial cells linked by tight junctions, encircled by astrocytic end-feet and pericytes leading to a selective barrier that determines the entry of molecules into the brain (10). This barrier represents in many instances a major obstacle for systemic brain metastasis treatment. Compounds that consist of more than eight to ten hydrogen bonds and are larger than 400–500 Da are prohibited from entering the brain. All large molecular drugs, such as antibodies, and 98% of small molecular drugs are excluded from the brain by the BBB (11). The brain is thus considered as a sanctuary site for metastatic growth (12) and the exposure to drugs is lower in brain metastases than systemic metastases. This is not only ascribed to the presence of the BBB but also the blood-tumor barrier (BTB) (13). The BTB differs from the BBB in that the vascular system is no longer surrounded by the other, normal BBB components, but tumor cells. Due to this structural difference, the BTB is proposed to be more permeable than the BBB (14). Micro-metastases, i.e. lesions smaller than 1 mm^3, usually have a lower permeability than larger metastases, in which the BTB might be compromised as a result of tumor growth (15).

Systemic therapy may therefore show efficacy on larger metastatic lesions, whereas micro-metastases receive subtherapeutic drug concentrations, which can contribute to treatment resistance (16). However, it has also been shown that there is not necessarily a straightforward association between brain metastasis size and drug uptake. Within the same lesion, the distribution can vary up to 10-fold (17). Also, melanoma patients with advanced disease can present with multiple brain metastases of different sizes with varying BTB integrities, further challenging systemic treatment (18). Several strategies have therefore been developed to temporarily disrupt the BBB for improved drug delivery such as focused ultrasound combined with circulating microbubble contrast agents (19-21), hyperosmotic opening (22-24) and radiotherapy (25). Other strategies involve the circumvention of the BBB by convection-enhanced delivery (26), viral-mediated or liposomal delivery (27), carrier molecules (28) and polymer wafers (29). These strategies have shown both strengths and weaknesses, but with limited success and many with apparent side effects (30,31).

It has previously been reported that the synthetic peptide K16ApoE can carry relatively large compounds into the mouse brain through the low-density lipoprotein receptor (LDLR) pathway (32). The use of K16ApoE in a therapeutic setting *in vivo*, however, has not been investigated. Here we determined, using advanced magnetic resonance imaging (MRI) techniques, the length of the therapeutic time window of K16ApoE BBB permeabilization in NOD/SCID mice and also its *in vivo* toxicity profile. Moreover, the morphological and functional effects of the peptide on cells and tissues were elucidated. In addition, we assessed the ability of K16ApoE to enhance drug delivery of a clinically active BRAFi (dabrafenib) on preclinical brain metastases, which was our main objective with this study. Finally, using PET/CT as an *in vivo* biodistribution tool for studying brain penetration, we assessed the potential of the peptide to deliver compounds to the brain with a size range corresponding to clinically relevant immune checkpoint inhibitors.

Materials and methods

K16ApoE peptide design and production

The K16ApoE peptide has the following amino acid sequence: KKKK-KKKK-KKKK-KKKK-LRVR-LASH-LRKL-RKRL-LRDA with a molecular weight (M_W) of 4 521.79 Da. The synthesis and characterization of the peptide is elaborated in Supplementary Materials. Briefly, a series of 16 lysine residues (K16) was covalently linked to the 20 amino acid part of the low-density lipoprotein receptor binding segment of apolipoprotein E (ApoE).

Cell culture

5 cell lines were used as constituents of the *in vitro* model system of the BBB, namely Mabin-Darby Canine Kidney (MDCK) cells, MDCK II, rat brain endothelial cells 4 (RBE4), human brain endothelial cells (hCMEC/D3) and human brain astrocytes (SC-1800). In addition, two brain metastatic melanoma cell lines were used; H1 (or H1_DL2) and H2. See Supplementary Materials. We obtained written consent by the Regional Ethical Committee (#013.09) and the Norwegian Directorate of Health (#9634) before human tumor tissue was collected and stored.

Animals

Female non-obese diabetic/severe combined immunodeficient (NOD/SCID) mice were purchased from Envigo (Gannat, France). The animals were bred and maintained in our animal facility certified by the Association for Assessment and Accreditation of Laboratory Animal Care International. They were fed a standard pellet diet and provided water *ad libitum*. Anaesthesia was induced with 3% sevoflurane (Abbott Laboratories Ltd., Berkshire, UK) in oxygen and maintained with 1.5% sevoflurane in oxygen during all procedures unless stated otherwise. The mice were monitored daily and sacrificed when significant morbidity symptoms were observed. The National

Animal Research Authority approved all animal procedures prior to all experiments (Application #8093, approved February 13th, 2016).

Evaluation of the *in vivo* toxicity of K16ApoE

The toxicity of K16ApoE was evaluated by intravenous tail vein injections of increasing concentrations of peptide into 38 NOD/SCID mice as described in Supplementary Materials and Supplementary Figure S1A.

Dynamic Contrast Enhanced Magnetic Resonance Imaging (DCE-MRI)

DCE-MRI was carried out using a 7 Tesla small-animal horizontal scanner (Bruker BioSpin GmbH, Ettlingen, Germany), using a 72 mm quadrature transmit coil and a 4-channel mouse brain array receive coil. The animals were placed in prone position and body temperature was maintained at 37 °C.

T_1 and T_2 weighted spin echo scans were acquired to provide anatomical references by using fast spin echo (FSE) protocols as described in Supplementary Materials. The mice received a dose of 50 (n=5), 100 (n=11) or 200 μg (n=5) of K16ApoE dissolved in 100 μL 9 mg/mL NaCl administered through the tail vein 10, 30, 60, 120 or 240 minutes before the start of the perfusion scans. Mice in the negative control group received 100 μL 9 mg/mL NaCl.

The perfusion scans were performed using dynamic contrast enhanced MRI (DCE-MRI) and analyzed using the Extended Tofts model implemented in nordicICE v2.3 (Nordic NeuroLab, Bergen, Norway) as described in Supplementary Materials.

Flow cytometry

RBE4 cells were pre-treated with 20 μg/mL rhodamine-conjugated K16ApoE for 45 minutes and exposed to inhibitors of dynamin- and clathrin-mediated endocytosis and studied by flow cytometry. RBE4, MDCK, hCMEC/D3, H1 and H2 cells were incubated with endocytosis

inhibitors and pre-treated with 20 μg/mL K16ApoE and Alexa Fluor 647-conjugated BSA prior to flow cytometry. Both experiments are elaborated in Supplementary Materials.

***In vitro* cell viability**

The viability of MDCK, MDCK II, RBE4 and hCMEC/D3 endothelial cells and H1 brain metastasis cells after treatment with K16ApoE was evaluated *in vitro* using a resazurin proliferation assay and for MDCK cells also a Live/Dead assay. The procedures are described in Supplementary Materials.

Scanning electron microscopy

RBE4 and MDCK II cells were incubated with 0, 20, 40 or 80 μg/mL K16ApoE for 45 minutes before they were fixed and prepared for scanning electron microscopy to study the morphology of the endothelial monolayers after peptide exposure. The protocol is described in Supplementary Materials.

***In vitro* human BBB models**

The procedure for the cell adhesion assay carried out prior to *in vitro* BBB modelling experimental set-ups is described in the Supplementary Materials.

Mono- and co-culture BBB models were constructed using the human astrocyte cell line SC-1800 and the endothelial cell line hCMEC/D3. The resistance values, indicating increased BBB permeability, were recorded using the Electric Cell Substrate Impedance Sensing (ECIS) system and CellZScope® for 2D and 3D modelling respectively, as reported previously (33). The mono- and co-cultures were treated with 0, 20, 40 or 80 μg/mL of K16ApoE and resistance was recorded until recovery of the barrier was observed. Resistance values were obtained in Ω from the ECIS system and $\Omega.cm^2$ from the automated sensing system, CellZScope®. See Supplementary Materials for a detailed description of the protocol.

In vivo biodistribution of ^{125}I–K16ApoE

To study the biodistribution of the peptide, we injected ^{125}I-K16ApoE intravenously into NOD/SCID mice and collected blood samples and a selection of organs and measured these for radioactivity. See Supplementary Materials for further details.

In vivo treatment study

In an initial control experiment, 9 NOD/SCID mice (8 weeks old) were injected with 5×10^5 H1_DL2 cells intracardially in 0.1 mL PBS as described in Supplementary Materials and divided into two groups by simple randomization: 4 animals were injected with 200 μg K16ApoE and 5 with 9 mg/mL NaCl, to exclude any treatment effects of the peptide.

36 female NOD/SCID mice (8 weeks old) were then injected with 5×10^5 H1_DL2 cells intracardially as described in Supplementary Materials. The next day, mice were by simple randomization divided into 3 treatment groups: The first group received 200 μg K16ApoE followed by 10 mg/kg dabrafenib (free base, CT-DABRF, ChemieTek, Indianapolis, IN, USA) 5 minutes later. The next group received 10 mg/kg dabrafenib and the third group received 9 mg/mL NaCl (vehicle).

All solutions were administered intravenously. The mice were treated twice a week for 6 weeks. See Supplementary Figure S1B for a detailed description of the animals used.

Contrast enhanced T_1 and T_2 weighted MRI was conducted 4 and 6 weeks after as described in Supplementary Materials.

Histology assessments

Mouse organs such as lungs, heart, liver, kidneys, colon, stomach, spleen, skin, muscle and brain were harvested after treatment with K16ApoE and fixed using 4% formaldehyde. Paraffin embedded organs were sectioned and mounted on slides. The sections were deparaffinized and stained with Hematoxylin and Eosin (H&E) for histological assessments.

Mass spectrometry

A mass spectrometry experiment was performed to confirm the presence of dabrafenib in K16ApoE combination treated NOD/SCID mice from the *in vivo* treatment experiment. The procedures are described in Supplementary Materials.

Dynamic PET/CT

The capacity of BBB permeability from K16ApoE was further evaluated by PET/CT using ^{18}F-albumin (~67 kDa) and ^{18}F-IgG (~150 kDa) to study if also these compounds could enter the brain after administration of K16ApoE. The albumin and IgG labelling procedure prior to PET/CT as well as the dynamic scanning procedures are described in Supplementary Materials.

Statistical analysis

The statistical analyses were carried out in Prism 7 for Mac, Version 7.0b (La Jolla, CA, USA). Unpaired t-tests were used to evaluate two normally distributed groups, whereas Mann-Whitney tests were used to compare nonparametric data. A Mantel-Cox log-rank test was used to analyze survival data from the *in vivo* treatment experiment. The results are displayed as individual points with mean ± SEM or mean ± SEM. A two-tailed *P*-value ≤0.05 was considered significant.

Results

Nontoxic doses of K16ApoE increase BBB permeability

To determine the maximum tolerated dose of K16ApoE, mice were injected intravenously with increasing concentrations of peptide (50 to 1,000 μg). For peptide doses up to 400 μg, the mice showed no signs of pain or distress following systemic peptide exposure, and they all recovered from anesthesia within approximately 3 minutes (Figure 1A). Higher peptide doses led to a respiratory and/or cardiac arrest within 30 minutes (Supplementary Videos 1 and 2). Higher doses were also associated with an abnormal erythrocyte morphology (Supplementary Figure S2).

K16ApoE facilitates a therapeutic window of minimum 30 minutes

DCE-MRI on healthy mice demonstrated a dose-dependent effect of the peptide. K16ApoE concentrations of 50 or 100 μg was insufficient for BBB permeabilization, i.e. allowing Omniscan to enter into the extravascular, extracellular space (EES) from the blood plasma, as seen by the K^{trans} values (Figure 1B). A major leakage of Omniscan contrast agent from blood into the brain tissue was observed when administered 10 minutes after injection of 200 μg K16ApoE. This implicates that the peptide was able to successfully open the intact BBB (Figure 1C, D). Interestingly, our results also showed that the BBB was partially open for up to approximately 1 hour after K16ApoE injection, reflecting a putative time frame for effective drug administration (Figure 1C, D). Other DCE-MRI parameters besides K^{trans} are listed in Supplementary Table 1. Based on the preceding, the toxicity studies above and previous literature (34), we chose to use 200 μg per mouse for further *in vivo* experiments.

Endocytic pathways are involved in cellular uptake of K16ApoE

To acquire a mechanistic insight on how K16ApoE facilitates BBB permeability, we first conducted baseline studies for further *in vitro* experiments. We determined K16ApoE IC_{50} values

for 5 normal endothelial cell lines, and these were all within a relatively narrow range of 30.89–86.18 μg/mL (Supplementary Figure S3A–D). For H1_DL2 cells used in the intracardiac metastasis model, the IC_{50} was 25.75 μg/mL (Supplementary Figure S3E).

Live/Dead assays and scanning electron microscopy images of MDCK and RBE4 cells (Supplementary Figure S3F-H) showed a dose/time-dependent increase in the number of dead cells over 45 minutes (see also Supplementary Videos 3-6).

We then applied flow cytometry to assess endocytic activity in RBE4 cells treated with 20 μg/mL rhodamine–labelled K16ApoE. As shown in Figure 2A, high endocytic uptake of peptide was observed in the RBE4 cells (pink curve in Figure 2A). By adding chlorpromazine (dark blue curve in Figure 2A) or dynasore (brown curve in Figure 2A), which are inhibitors of clathrin and dynamin mediated endocytosis, respectively, the peptide uptake was reduced with the strongest effect seen for chlorpromazine.

We then pre-treated RBE4 cells with AF647-labeled BSA and incubated with (purple curve in Figure 2B) and without K16ApoE (green curve in Figure 2B). When chlorpromazine was added as well, there was a reduction in BSA uptake (black curve in Figure 2B). The lowest BSA uptake was seen in RBE4 cells incubated with chlorpromazine and no peptide (yellow curve in Figure 2B). Corresponding experiments were carried out on MDCK, hCMEC/D3, H1 and H2 cells studying BSA uptake after pre-treatment with endocytosis inhibitors (Supplementary Figure 4). The same pattern was seen across all cell lines: The highest BSA uptake was observed for cells pretreated with K16ApoE (purple curves), whereas endocytosis inhibitors reduced this increase, chlorpromazine (yellow curves) to a larger extent than dynasore (blue curves). Dynamin-mediated endocytosis can be serum dependent. We therefore carried out the dynasore experiments with (Supplementary Figure S4) and without BSA (Figure 2). To summarize, both clathrin- and dynamin-mediated endocytosis are likely involved in K16ApoE uptake (below IC_{50}-doses).

In order to show that also other uptake mechanisms of K16ApoE likely are involved, we investigated the uptake of AF647-conjugated BSA in RBE4 cells with (purple curves in Fig 2C and

2D) and without (green curves in Fig 2C and 2D) pre-treatment with K16ApoE. When compared to 37 °C, the uptake of BSA was reduced in cells that were kept at 4° C (Figure 2D), i.e. at a temperature when endocytosis usually is abolished (Figure 2C). In conclusion, based on the above data, endocytic mechanisms are involved in peptide uptake, likely in combination with other mechanisms as described in the following.

K16ApoE has lytic properties at higher concentrations (above IC_{50})

We then studied changes in endothelial cell monolayer surfaces *in vitro* following K16ApoE exposure. Scanning electron microscopy images showed that MDCK II and RBE4 cells not exposed to the peptide formed uniform monolayers (Figure 3A and Supplementary Figure S3H, respectively) with occasional protruding cells with smooth surfaces. At increasing K16ApoE concentrations, the cell surface lost the uniform morphology, and punctures in the membranes could be observed, indicating dying cells (See inserts in Figure 3A). There was an association between increasing concentrations of the peptide and the number of punctured, protruding cells. This dose-dependent cell death was verified by the Live/Dead experiment (Figure 3B and Supplementary Figure S3F and G).

Taken together with data presented in Supplementary Figure S2 and S3, this indicates that cell lysis is likely involved especially at higher peptide concentrations, likely due to a cationic effect leading to electrostatic interactions with negatively charged cell membranes (35), in addition to the endocytosis mechanisms indicated by flow cytometry (Figure 2).

BBB integrity is restored 15 hours after treatment with the peptide

Cellular adhesion was measured prior to *in vitro* BBB modelling using crystal violet in 96-well plates after treatment with 0, 20, 40 or 80 μg/mL K16ApoE for 45 minutes. The strongest cellular adhesion was observed for untreated hCMEC/D3 cells. The adhesion potential was significantly reduced during peptide treatment in a dose-dependent manner (Supplementary Figure

S5A and B). However, although not statistically significant, there was a tendency that the adhesion potential started to recover with increasing recovery times after 45 minutes of peptide exposure. Endothelial cells exposed to 40 and 80 µg/mL showed a statistically significant increase in adhesion potential after 60 minutes (Supplementary Figure S5A).

In both human *in vitro* BBB models assessed, the cells were exposed to 0, 20, 40 or 80 µg/mL of the peptide for 45 minutes, before they were allowed to recover for as long as deemed necessary in a mono- and co-culture model. In the mono-culture model, the endothelial cell monolayers restored their integrity within 3 hours (Figure 3C), whereas in the co-culture model with endothelial cells and astrocytes, the integrity of both cell layers was restored after 15 hours (Figure 3D).

K16ApoE is eliminated from blood plasma within five minutes, through liver, kidney and spleen

The activity of ^{125}I-labeled K16ApoE in blood plasma was rapidly reduced over the total measured time of 30 minutes. The most prominent decline was observed within the first minute after the peptide was injected into the tail vein, whereas subsequent values quickly reached a baseline. The curve corresponds to a half-life of K16ApoE in blood of approximately 1 minute (Supplementary Figure S6B).

The biodistribution of ^{125}I-K16ApoE was analysed in numerous selected organs. The highest values of ^{125}I-K16ApoE accumulation were seen in the liver (164 570 cpm), kidney (160 107 cpm) and spleen (136 889 cpm), whereas the lowest counts were observed in colon (17 290 cpm), femur (14 720 cpm) and muscle tissue (13 608 cpm). Intermediate values were observed for ventricle (92 533 cpm), lungs (76 554 cpm), skin (38 835 cpm) and heart (28 482 cpm). The high activity seen in the kidneys, liver and spleen suggested that elimination occurred through all of these organs (Supplementary Figure S6C).

Since ^{125}I was labelled to the only histidine residue present in the peptide, the potency of the final ^{125}I-K16ApoE construct only allowed us to inject a concentration of 25 μg K16ApoE without exceeding the maximum volume possible to inject intravenously in a NOD/SCID mouse. Further, since the measurements were carried out more than 30 minutes after the peptide was injected, this is a time window that does not allow major remnants of the peptide to be detected in the brain. For these reasons combined, we did not focus on the amount of peptide in the brain in this experiment, as both the concentration and time window likely is too small to see any significant uptake, as observed by DCE-MRI (Figure 1).

K16ApoE does not induce acute or long-term tissue damage

Histological analysis was carried out in two separate experiments (Supplementary Figure S1). In the first experiment, healthy NOD/SCID mice were subjected to a one-time exposure of 0, 200, 400, 600, 800 or 1 000 μg K16ApoE (Supplementary Figure S7A). In the second experiment, tumor-bearing animals were subjected to 200 μg K16ApoE twice a week over a period of six weeks (Supplementary Figure S7B). Representative H&E sections from brain, lungs, kidneys, liver, spleen, skin, muscle tissue, colon, stomach and heart did not reveal any pathological changes in animals from either treatment group, across both experiments (Supplementary Figures S7A and B).

K16ApoE improves the delivery of the BRAFi dabrafenib

We then studied whether a combined use of K16ApoE with dabrafenib (537.6 Da) could increase the therapeutic effects in a human brain metastasis animal model, compared to dabrafenib treatment alone.

A small control experiment was initially carried out with injections of only K16ApoE or vehicle (saline) to evaluate whether the peptide itself had any therapeutic effects on tumor burden. No such effects were observed (Supplementary Figure S8A–C). A larger study was then done with

three treatment groups: Dabrafenib, K16ApoE and dabrafenib and vehicle. In order to minimize the number of animals used, the K16ApoE alone group was not repeated.

The mean number of tumors as well as the mean total tumor volume in animals treated with a combination of K16ApoE and dabrafenib decreased at weeks 4 and 6, compared to control animals (vehicle) or animals treated with dabrafenib only (Figure 4A–C). No statistically significant differences could be found in tumor numbers or tumor volumes between the dabrafenib group and the control group at week 4 and 6, indicating that dabrafenib treatment alone was not effective.

Kaplan-Meier curves revealed no difference in survival between vehicle and dabrafenib treated animals whereas the combinatorial treatment group had a significant survival benefit (Figure 4D).

K16ApoE treatment causes an uptake of dabrafenib in the brain parenchyma

A pilot mass spectrometry imaging experiment revealed that dabrafenib was taken up in the brain in mice treated with a co-injection of peptide and dabrafenib, as shown in Supplementary Figure S9A. A negative control animal treated with vehicle is presented in Supplementary Figure S9B, where no uptake is detected. Dabrafenib was fragmented in two segments, namely at m/z 480.1 and 344.1 as seen in Supplementary Figure S9C.

K16ApoE facilitates blood-brain barrier penetration of large molecules

To test the potential of K16ApoE to carry even larger molecules than dabrafenib across the BBB, we injected 200 μg K16ApoE followed by ^{18}F-albumin (~67 kDa) or ^{18}F-IgG (~150 kDa) and performed subsequent dynamic PET/CT brain imaging. Over 30–60 minutes, we observed a significant increase in average standardized uptake values (SUV_{mean}) in peptide–injected mice as compared to vehicle–treated mice for both ^{18}F-albumin (Figure 5A) and ^{18}F-IgG (Figure 5B). This implies leakage of the radiolabeled molecules from the blood plasma and into the EEC. Thus, K16ApoE facilitates the delivery of compounds with a molecular weight of up to at least 150 kDa.

Discussion

The delivery of therapeutic drug concentrations across the BBB and into metastatic lesions remains a critical issue in the treatment of brain metastases. In the smallest lesions not detected by clinical MRI, the BBB is presumably intact. As the brain metastases progress, the barriers develop a heterogeneous permeability to different-sized molecules, still with many metastases showing minor or no permeability at all (15). Thus, efficient drug delivery to the brain lesions is often compromised, necessitating the need for strategies to increase the leakiness of the BBB (30). Here, we describe a treatment strategy using a BBB permeabilizing peptide and thereby improving the delivery of dabrafenib (537.6 Da), which previously has demonstrated profound effects towards extracranial melanomas with BRAF mutations. Although the anatomical distribution of dabrafenib is superior to several other BRAFis (9), the drug does not readily penetrate into the brain parenchyma if the BBB is intact. Here we show that our treatment strategy inhibits the progression of $BRAF^{V600E}$ mutated melanoma brain metastases, ascribed to an improved drug delivery across the BBB.

In a previous study with K16ApoE, Evans blue (M_W ~0.96 kDa) was injected 10 minutes after administering the peptide, and the results indicated that a therapeutic window of approximately 60 minutes was facilitated (34). We used DCE-MRI which is a quantitative and highly sensitive MRI technique to validate these results. The observed increase in K^{trans} values demonstrates a genuine pharmacodynamic increase in BBB permeability and thus perfusion (36), and this was directly attributable to peptide action.

However, although it has been shown by us and others that K16ApoE is able to permeabilize the BBB, the specific mechanisms responsible for this effect have not been firmly established (32,34,37). Meng and colleagues have previously seen that K16ApoE likely promotes endocytosis into endothelial cells (37). Our findings indicate that there are likely several mechanisms involved, including loss in cell membrane integrity and lytic properties in addition to endocytosis, especially at higher peptide concentrations. We show that the cellular uptake of

K16ApoE at lower doses (i.e. 20 μg/mL) was reduced by dynasore and chlorpromazine, inhibitors of dynamin-dependent and clathrin-mediated endocytosis, respectively. Our data may suggest that clathrin-mediated endocytosis is the most active one of these two mechanisms, which is also in line with the literature (38). We found that peptide-mediated uptake of BSA was still present at low temperatures (4 °C) when endocytosis is significantly reduced, although at reduced levels. This adds to the hypothesis that also other cellular uptake-mechanisms may be involved. For instance, our scanning electron microscopy data indicated that the peptide exerted a dose-dependent, toxic effect on the cells, which has also been reported previously (37). At increasing concentrations, more cells with punctured cell membranes were observed (Figure 3A), suggesting also a lytic effect at higher concentrations. These findings were supported by our fluorescence time lapse study, which also indicated that the cells were relatively unaffected by the peptide during the first minute of exposure. In addition, the half-life of K16ApoE in the blood was approximately one minute, which taken together implies that relatively large doses of peptide (above the IC_{50} doses) may be injected safely into the bloodstream. This is also supported by the *in vivo* toxicity study summarized in Figure 1A.

The endothelial cell integrity after exposure to the peptide was studied using *in vitro* BBB models and by investigating peptide action on proteins important in the assembly and maintenance of tight junctions. The peptide reduced the endothelial barrier integrity as measured using both ECIS (Figure 3C) and cellZScope (Figure 3D). Within 3 hours, the endothelial monolayer was restored, whereas the co-culture system remodelled the barrier integrity after 15 hours. This time discrepancy may be explained based on the fact that the methods are not directly comparable to each other. In the ECIS system, the output values are normalized before the resistance values can be regarded as absolute, while the measured resistance in cellZscope is directly attributable to the cell layers. Also, in the ECIS measurements there was only one layer of cells while a co-culture was constructed for the cellZScope. Thus, both cell lines had to recover for the barrier to be intact. Nevertheless, the results from both systems indicate that the BBB is restored after being transiently

exposed to K16ApoE. In addition to its added mechanistic information, these experiments also validate the peptide action in a 3D human system.

In the *in vivo* treatment study summarized in Figure 4, 200 μg K16ApoE was administered intravenously into each mouse, and with a blood volume of approximately 1.5 mL, this corresponds to a peptide concentration of around 133 μg/mL blood. No side effects were observed after these injections, presumably due to the quick clearance from the blood, which occurred mainly through the liver, spleen and kidneys. Meng and colleagues argued that there was a positive correlation between toxic effects of the peptide at higher concentrations and BBB permeabilization. They also indicated that interactions of the peptide with adjacent erythrocytes resulted in the formation of microthrombi, which could be the underlying mechanism of toxicity (37). Taken together with our findings of hemolysis after treatment with K16ApoE, the injection of 200 μg K16ApoE per mouse thus represents a compromise between a favorable BBB permeable effect of the peptide and potential unwanted toxic side effects.

Our drug delivery strategy involved intravenous administration of a drug that normally is given orally to patients, thus several potential effects on the drug from the gastrointestinal tract such as degrading enzymes, low pH or heterogenous blood perfusion were not taken into consideration. We also administered 10 mg/kg to the mice twice a week, while in the clinic, patients are commonly given 2 × 150 mg dabrafenib daily, which corresponds to 4 mg/kg for a 75 kg patient. Although the concentrations are not directly comparable, our findings clearly suggest that dabrafenib represents an effective treatment for melanoma brain metastases, provided successful entry through the BBB. The amount of injected drug that penetrated the BBB and accumulated within the mouse brains was not quantified. However, a pilot mass spectrometry experiment of brain tissue harvested from control mice and K16ApoE + dabrafenib treated mice was performed, showing the presence of dabrafenib within the brains after peptide administration. Dabrafenib was not found in brains from control mice. Further experiments should be carried out aiming to quantify the detected amount of drug when co-injected with K16ApoE.

The histopathological examination performed by an experienced neuropathologist showed that no changes in organ histology could be found after administering a single high-dose (1,000 μg) of peptide to the mice, or at the end of the dabrafenib study, when the mice had been given 12 injections of 200 μg K16ApoE over six weeks.

As a final experiment, we used dynamic PET/CT to study whether the BBB was permeable, following K16ApoE exposure, to even larger molecules. We detected ^{18}F-labelled albumin (M_W ~67 kDa) and IgG (M_W ~150 kDa) in brain tissue. Although drug uptake across the BBB or BTB is not only limited to size, our results indicate that K16ApoE can facilitate the delivery of substances in the size range of immune checkpoint inhibitors to patients with brain metastases. Examples include ipilimumab (M_W ~148 kDa), which targets cytotoxic T-lymphocyte antigen 4 (CTLA4) or inhibitors of PD-1/PD-L1 such as for instance nivolumab (M_W ~143 kDa) and atezolizumab (M_W ~145 kDa), respectively. Thus, for future investigations, we aspire to carry out *in vivo* treatment experiments with immune checkpoint inhibitors on melanoma brain metastases.

In conclusion, the use of K16ApoE seems to be a promising strategy to improve drug delivery across the BBB. Potential toxicity issues preclude direct translation into the clinic as of today, warranting further studies with the peptide, which is also the case with several other methods of permeabilizing the BBB. Our strategy using K16ApoE serves as an easy, non-invasive and reliable tool to establish treatment effects *in vivo* with agents that otherwise do not penetrate the BBB.

Acknowledgements

The authors thank Hege Avsnes Dale (Molecular Imaging Center, University of Bergen) for valuable assistance with confocal and light microscopy, Anne Karin Nyhaug (Molecular Imaging Center, University of Bergen) for help with tissue sample preparation before electron microscopy, Linda Sandven (Molecular Imaging Center, University of Bergen) for H&E staining, Miro Eigenmann (Institute of Biomedicine, University of Bergen) for input on the development of the biodistribution methodology, Mari-Ann Jørstad Davidsen (Department of Clinical Medicine, University of Bergen) for help with animal procedures, Brith Bergum (Department of Clinical Science, University of Bergen) for assistance with flow cytometry, Jubayer Hossain (The Department of Biomedicine, University of Bergen) for assistance with animal work, Marjo Yliperttula (University of Helsinki) for providing us MDCK II cells, Tilo Wolf Eichler (Department of Clinical Medicine, University of Bergen) for providing us MDCK cells, Michael Aschner (Vanderbilt University) for the RBE4 cells, Tom Christian Holm Adamsen (Department of Chemistry, University of Bergen) for valuable input on PET/CT methodology, Tina Pavlin (Molecular Imaging Center, University of Bergen) for help with the MRI.

The electron microscopy, confocal and small animal imaging was performed at the Molecular Imaging Center, Department of Biomedicine, University of Bergen.

The study was funded by the Western Norway Regional Health Authority (F. Thorsen), the Kristian Gerhard Jebsen Foundation (R. Bjerkvig), the Norwegian Cancer Society (F. Thorsen), Animal Free Research UK (G. Pilkington) and Brain Tumor Research (G. Pilkington).

Authors contributions

Concept and design: S.N. Aasen, D.E. Olberg, G. Pilkington, G. Sarkar, R.B. Jenkins, T. Sundstrøm, R. Bjerkvig and F. Thorsen.

Development of methodology: S.N. Aasen, H. Espedal, O. Keunen, O. Tenstad, A.V. Eikeland, H. Baghirov, G. Pilkington, R. Bjerkvig and F. Thorsen

Acquisition of data: S.N. Aasen, H. Espedal, C.F. Holte, O. Keunen, T.V. Karlsen, Z. Maherally, T. Hoang, A.V. Eikeland, H. Baghirov and F. Thorsen

Analysis and interpretation of data: S.N. Aasen, H. Espedal, C.F. Holte, O. Keunen, Z. Maherally, H. Miletic, T. Hoang, A.V. Eikeland, H. Baghirov and F. Thorsen.

Writing, review and/or revision of the manuscript: S.N. Aasen, Z. Maherally, G. Pilkington, T. Sundstrøm, R. Bjerkvig and F. Thorsen.

Study supervision: R. Bjerkvig and F. Thorsen.

References

1. Owonikoko TK, Arbiser J, Zelnak A, Shu HK, Shim H, Robin AM*, et al.* Current approaches to the treatment of metastatic brain tumours. Nat Rev Clin Oncol **2014**;11(4):203-22 doi 10.1038/nrclinonc.2014.25.

2. Sinik L, Minson KA, Tentler JJ, Carrico J, Bagby SM, Robinson WA*, et al.* Inhibition of MERTK Promotes Suppression of Tumor Growth in BRAF Mutant and BRAF Wild-Type Melanoma. Mol Cancer Ther **2019**;18(2):278-88 doi 10.1158/1535-7163.MCT-18-0456.

3. Grzywa TM, Paskal W, Wlodarski PK. Intratumor and Intertumor Heterogeneity in Melanoma. Transl Oncol **2017**;10(6):956-75 doi 10.1016/j.tranon.2017.09.007.

4. Villar-Prados A, Wu SY, Court KA, Ma S, LaFargue C, Chowdhury MA*, et al.* Predicting Novel Therapies and Targets: Regulation of Notch3 by the Bromodomain Protein BRD4. Mol Cancer Ther **2019**;18(2):421-36 doi 10.1158/1535-7163.MCT-18-0365.

5. Heller KN, Pavlick AC, Hodi FS, Thompson JA, Margolin KA, Lawrence DP*, et al.* Safety and survival analysis of ipilimumab therapy in patients with stable asymptomatic brain metastases. Journal of Clinical Oncology **2011**;29:8581– doi 10.1200/jco.2011.29.15_suppl.8581.

6. Kluger HM. Safety and activity of pembrolizumab in melanoma patients with untreated brain metastases. Journal of Clinical Oncology **2015**;33:9009 doi 10.1200/jco.2015.33.15_suppl.9009.

7. Long GV, Trefzer U, Davies MA, Kefford RF, Ascierto PA, Chapman PB*, et al.* Dabrafenib in patients with Val600Glu or Val600Lys BRAF-mutant melanoma metastatic to the brain (BREAK-MB): a multicentre, open-label, phase 2 trial. Lancet Oncol **2012**;13(11):1087-95 doi 10.1016/S1470-2045(12)70431-X.

8. Eichler AF, Chung E, Kodack DP, Loeffler JS, Fukumura D, Jain RK. The biology of brain metastases-translation to new therapies. Nat Rev Clin Oncol **2011**;8(6):344-56 doi 10.1038/nrclinonc.2011.58.

9. Mittapalli RK, Vaidhyanathan S, Dudek AZ, Elmquist WF. Mechanisms limiting distribution of the threonine-protein kinase B-RaF(V600E) inhibitor dabrafenib to the brain: implications for the treatment of melanoma brain metastases. J Pharmacol Exp Ther **2013**;344(3):655-64 doi 10.1124/jpet.112.201475.

10. Weidle UH, Niewohner J, Tiefenthaler G. The Blood-Brain Barrier Challenge for the Treatment of Brain Cancer, Secondary Brain Metastases, and Neurological Diseases. Cancer Genomics Proteomics **2015**;12(4):167-77.

11. Pardridge WM. The blood-brain barrier: bottleneck in brain drug development. NeuroRx **2005**;2(1):3-14 doi 10.1602/neurorx.2.1.3.

12. Palmieri D, Chambers AF, Felding-Habermann B, Huang S, Steeg PS. The biology of metastasis to a sanctuary site. Clin Cancer Res **2007**;13(6):1656-62 doi 10.1158/1078-0432.CCR-06-2659.

13. Lin X, DeAngelis LM. Treatment of Brain Metastases. J Clin Oncol **2015**;33(30):3475-84 doi 10.1200/JCO.2015.60.9503.

14. Terrell-Hall TB, Ammer AG, Griffith JI, Lockman PR. Permeability across a novel microfluidic blood-tumor barrier model. Fluids Barriers CNS **2017**;14(1):3 doi 10.1186/s12987-017-0050-9.

15. Thorsen F, Fite B, Mahakian LM, Seo JW, Qin S, Harrison V*, et al.* Multimodal imaging enables early detection and characterization of changes in tumor permeability of brain metastases. J Control Release **2013**;172(3):812-22 doi 10.1016/j.jconrel.2013.10.019.

16. Seoane J, De Mattos-Arruda L. Brain metastasis: new opportunities to tackle therapeutic resistance. Mol Oncol **2014**;8(6):1120-31 doi 10.1016/j.molonc.2014.05.009.

17. Samala R, Thorsheim HR, Goda S, Taskar K, Gril B, Steeg PS*, et al.* Vinorelbine Delivery and Efficacy in the MDA-MB-231BR Preclinical Model of Brain Metastases of Breast Cancer. Pharm Res **2016**;33(12):2904-19 doi 10.1007/s11095-016-2012-3.

18. Khuntia D, Brown P, Li J, Mehta MP. Whole-brain radiotherapy in the management of brain metastasis. J Clin Oncol **2006**;24(8):1295-304 doi 10.1200/JCO.2005.04.6185.

19. Hynynen K, McDannold N, Vykhodtseva N, Jolesz FA. Noninvasive MR imaging-guided focal opening of the blood-brain barrier in rabbits. Radiology **2001**;220(3):640-6 doi 10.1148/radiol.2202001804.

20. McDannold N, Arvanitis CD, Vykhodtseva N, Livingstone MS. Temporary disruption of the blood-brain barrier by use of ultrasound and microbubbles: safety and efficacy evaluation in rhesus macaques. Cancer Res **2012**;72(14):3652-63 doi 10.1158/0008-5472.CAN-12-0128.

21. Alkins R, Burgess A, Ganguly M, Francia G, Kerbel R, Wels WS*, et al.* Focused ultrasound delivers targeted immune cells to metastatic brain tumors. Cancer Res **2013**;73(6):1892-9 doi 10.1158/0008-5472.CAN-12-2609.

22. Rapoport SI, Hori M, Klatzo I. Testing of a hypothesis for osmotic opening of the blood-brain barrier. Am J Physiol **1972**;223(2):323-31 doi 10.1152/ajplegacy.1972.223.2.323.

23. Neuwelt EA, Barnett PA, Hellstrom I, Hellstrom KE, Beaumier P, McCormick CI*, et al.* Delivery of melanoma-associated immunoglobulin monoclonal antibody and Fab fragments to normal brain utilizing osmotic blood-brain barrier disruption. Cancer Res **1988**;48(17):4725-9.

24. Liu LB, Xue YX, Liu YH. Bradykinin increases the permeability of the blood-tumor barrier by the caveolae-mediated transcellular pathway. J Neurooncol **2010**;99(2):187-94 doi 10.1007/s11060-010-0124-x.

25. Cao Y, Tsien CI, Shen Z, Tatro DS, Ten Haken R, Kessler ML*, et al.* Use of magnetic resonance imaging to assess blood-brain/blood-glioma barrier opening during conformal radiotherapy. J Clin Oncol **2005**;23(18):4127-36 doi 10.1200/JCO.2005.07.144.

26. Bobo RH, Laske DW, Akbasak A, Morrison PF, Dedrick RL, Oldfield EH. Convection-enhanced delivery of macromolecules in the brain. Proc Natl Acad Sci U S A **1994**;91(6):2076-80.

27. Gupta B, Levchenko TS, Torchilin VP. TAT peptide-modified liposomes provide enhanced gene delivery to intracranial human brain tumor xenografts in nude mice. Oncol Res **2007**;16(8):351-9.

28. Saenz del Burgo L, Hernandez RM, Orive G, Pedraz JL. Nanotherapeutic approaches for brain cancer management. Nanomedicine **2014**;10(5):905-19 doi 10.1016/j.nano.2013.10.001.

29. Bregy A, Shah AH, Diaz MV, Pierce HE, Ames PL, Diaz D*, et al.* The role of Gliadel wafers in the treatment of high-grade gliomas. Expert Rev Anticancer Ther **2013**;13(12):1453-61 doi 10.1586/14737140.2013.840090.

30. Azad TD, Pan J, Connolly ID, Remington A, Wilson CM, Grant GA. Therapeutic strategies to improve drug delivery across the blood-brain barrier. Neurosurg Focus **2015**;38(3):E9 doi 10.3171/2014.12.FOCUS14758.

31. Shawkat H, Westwood M-M, Mortimer A. Mannitol: a review of its clinical uses. Continuing Education in Anaesthesia Critical Care & Pain **2012**;12(2):82-5 doi 10.1093/bjaceaccp/mkr063.

32. Sarkar G, Curran GL, Mahlum E, Decklever T, Wengenack TM, Blahnik A*, et al.* A carrier for non-covalent delivery of functional beta-galactosidase and antibodies against amyloid plaques and IgM to the brain. PLoS One **2011**;6(12):e28881 doi 10.1371/journal.pone.0028881.

33. Maherally Z, Fillmore HL, Tan SL, Tan SF, Jassam SA, Quack FI*, et al.* Real-time acquisition of transendothelial electrical resistance in an all-human, in vitro, 3-dimensional, blood-brain barrier model exemplifies tight-junction integrity. FASEB J **2018**;32(1):168-82 doi 10.1096/fj.201700162R.

34. Sarkar G, Curran GL, Sarkaria JN, Lowe VJ, Jenkins RB. Peptide carrier-mediated non-covalent delivery of unmodified cisplatin, methotrexate and other agents via intravenous route to the brain. PLoS One **2014**;9(5):e97655 doi 10.1371/journal.pone.0097655.

627 35. Szczepanski C, Tenstad O, Baumann A, Martinez A, Myklebust R, Bjerkvig R*, et al.*
628 Identification of a novel lytic peptide for the treatment of solid tumours. Genes Cancer **2014**;5(5-
629 6):186-200.
630 36. Barrett T, Brechbiel M, Bernardo M, Choyke PL. MRI of tumor angiogenesis. J Magn
631 Reson Imaging **2007**;26(2):235-49 doi 10.1002/jmri.20991.
632 37. Meng Y, Wiseman JA, Nemtsova Y, Moore DF, Guevarra J, Reuhl K*, et al.* A Basic ApoE-
633 Based Peptide Mediator to Deliver Proteins across the Blood-Brain Barrier: Long-Term Efficacy,
634 Toxicity, and Mechanism. Mol Ther **2017**;25(7):1531-43 doi 10.1016/j.ymthe.2017.03.037.
635 38. García-Ruiz C, Ribas V, Baulies A, Fernández-Checa JC. Mitochondrial Cholesterol and the
636 Paradox in Cell Death. In: Singh H, Sheu SS, editors. Pharmacology of Mitochondria Handbook of
637 Experimental Pharmacology. Volume 240. Switzerland: Springer International Publishing; 2016.
638
639
640

Figure legends

Figure 1

K16ApoE creates a time window for therapy for at least 30 minutes. **A,** Survival curves after K16ApoE dose escalation experiments. **B,** Scatter plots of the blood-to-tissue transfer constant (K^{trans}) demonstrate a dose-dependent reduction of contrast agent transfer from blood to tissue with decreasing peptide concentrations (n=5-10 mice). Mean ± SEM. **C,** Representative anatomical contrast enhanced T_1 weighted MR images (top row) and parametric MR images (K^{trans} and AUC maps; two bottom rows) of coronal brain sections of a control mouse are seen to the left. Scalebar = 2.5 mm. **D**, the quantified K^{trans} analysis demonstrates leakage of contrast agent from blood to tissue 10 and 30 minutes after injection of 200 µg of K16ApoE, compared to control animals (n=5-10 mice). Mean ± SEM. Abbreviations**:** K^{trans}: transfer constant, T_1CE: contrast enhanced T_1 weighted scan, AUC: area under curve, **: $p < 0.01$.

Figure 2

Mechanistic studies of the *in vitro* effects of K16ApoE. **A,** Flow cytometry data showing the effects of two endocytosis inhibitors, chlorpromazine and dynasore after 30 minutes of incubation, on K16ApoE uptake in RBE4 cells after 45 minutes of continued incubation. **B,** Flow cytometry data on uptake of BSA into cells while pre-treating RBE4 cells with chlorpromazine for 30 minutes, with and without using the peptide for 45 minutes. **C,** Flow cytometry data showing uptake of BSA at 37 °C and at **D,** 4 °C after incubating the cells for one hour. Abbreviations: RBE4: rat brain endothelial cells 4, BSA: bovine serum albumin, cp: chlorpromazine.

Figure 3

Integrity of an *in vitro* model of the blood-brain barrier after exposure to the peptide. **A,** Scanning electron microscopy images demonstrating nonspecific cell monolayer disruptions in preparations

of MDCK II cells. Inserts in micrographs with cells exposed to 0 µg/mL K16ApoE demonstrate smooth cell membranes, whereas cells exposed to 80 µg/mL of the peptide have punctured cell membranes. All scalebars 20 µm. **B,** Cell death as a result of corresponding peptide concentrations as seen by Live/Dead staining of MDCK cells. Scalebar 50 µm. **C,** Recorded resistance values using the ECIS system in a monolayer of hCMEC/D3 endothelial cells. The resistance was restored 3 h after peptide exposure. **D,** Measured resistance (TEER) values using the CellZScope system in a co-culture consisting of astrocytes and hCMEC/D3 endothelial cells. Barrier integrity was restored 15 h after peptide exposure. Cell illustration from Somersault1824 (www.somersault1824.com). Abbreviations: ECIS: Electric cell substrate impedance sensing, TEER: transendothelial/epithelial electrical resistance.

Figure 4

Combined treatment with K16ApoE and dabrafenib inhibits tumor development and increases animal survival in an animal model of melanoma brain metastasis. **A,** The mean, total number of tumors in the mouse brains four (left) and six (right) weeks after start of treatment. Mann-Whitney statistical test. Mean ± SEM. **B,** The mean, total tumor volumes in the mouse brains four (left) and six (right) weeks after start of treatment. Mean ± SEM. **C,** Representative CE T_1 weighted and T_2 weighted MR images from each treatment group at week four and six. Scalebar 2 mm. **D,** Survival curves for all animals in the treatment study. Abbreviations: *: $p<0.05$, **: $p<0.01$, ****: 0.0001, CE T_1: contrast enhanced T_1 weighted MR images obtained 5 minutes after injection of Omniscan, T_2: T_2 weighted MR images.

Figure 5

K16ApoE facilitates the delivery of large compounds across the BBB. **A,** Standardized uptake of ^{18}F-albumin into brain tissue, monitored by a 30 minutes dynamic PET/CT scan. Each mouse was scanned twice, with and without a prior injection of 200 µg K16ApoE, on separate days (n=3 mice).

The mean standard uptake value (SUV_{mean}) was calculated within an ellipsoidal volume of interest, delineating the skull. Mean ± SEM. **B,** Standardized uptake of ^{18}F-IgG into brain tissue, monitored by a 60 minutes dynamic PET/CT scan. Each mouse was scanned twice, with and without a prior injection of 200 µg K16ApoE, on separate days (n=7 mice). The mean standard uptake value (SUV_{mean}) was calculated. Mean ± SEM. Abbreviations: SUV: standardized uptake values, ^{18}F: Fluorine-18, PET: positron emission tomography, IgG: immunoglobulin G, *: $p<0.05$.

Figure 1

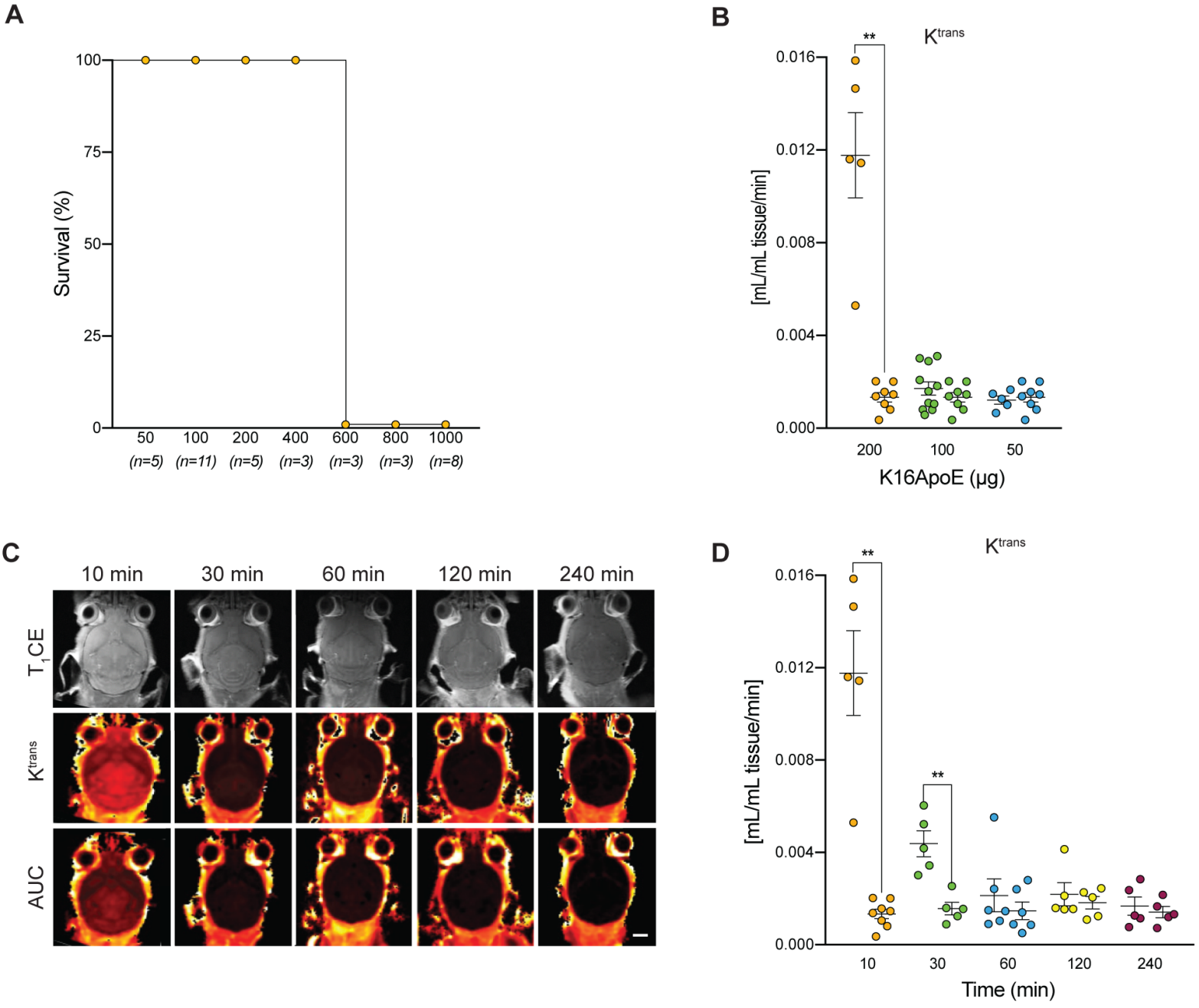
A
100
75
50
25
0
Survival (%)
50
100
200
400
600
800
1000
(n=5)
(n=11)
(n=5)
(n=3)
(n=3)
(n=3)
(n=8)
B
**
K trans
0.016
0.012
0.008
0.004
0.000
[mL/mL tissue/min]
200
100
50
K16ApoE (µg)
C
10 min
30 min
60 min
120 min
240 min
T1CE
K trans
AUC
D
**
**
K trans
0.016
0.012
0.008
0.004
0.000
[mL/mL tissue/min]
10
30
60
120
240
Time (min)

Figure 2

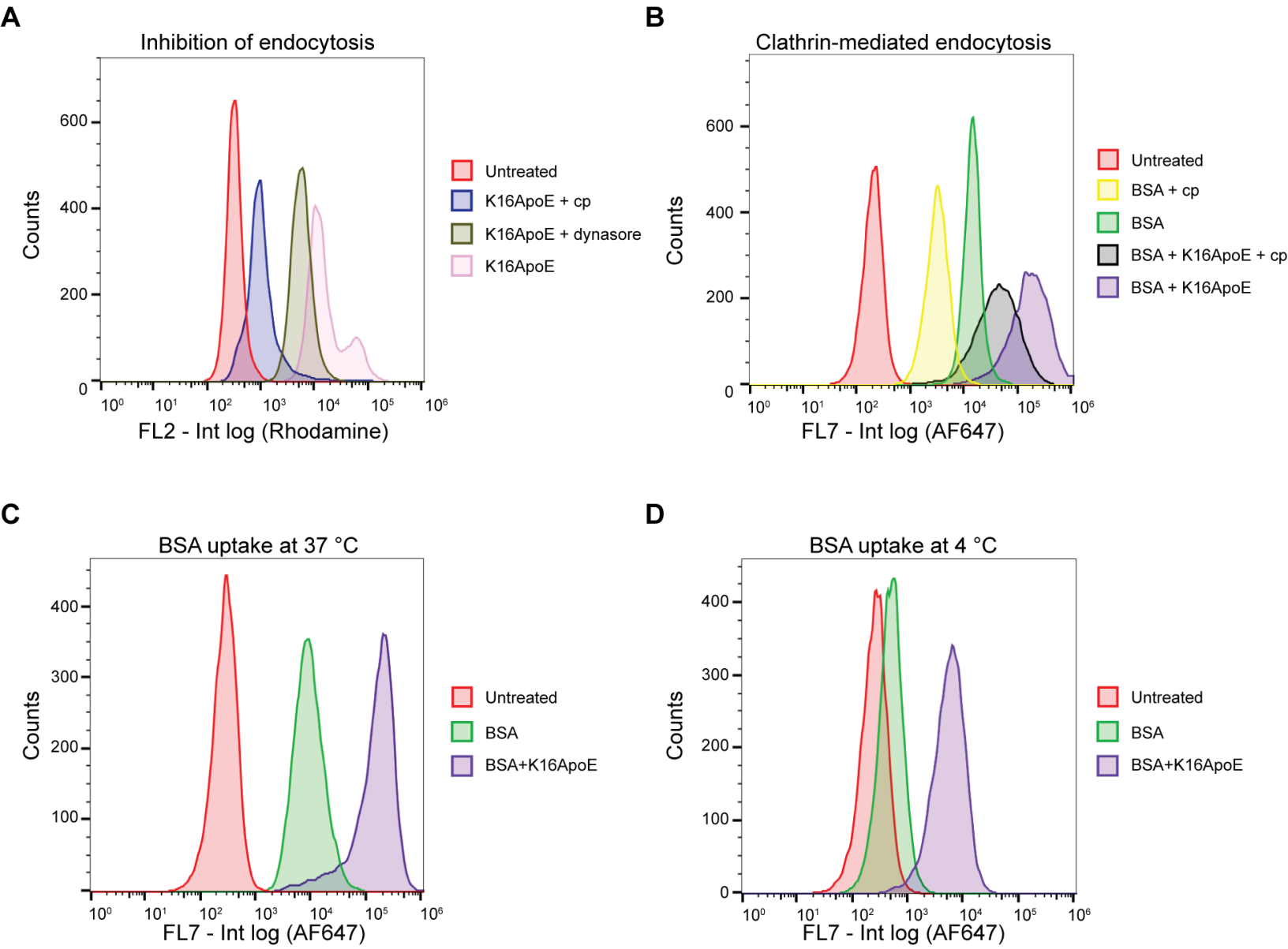
A
Inhibition of endocytosis
Counts
FL2 - Int log (Rhodamine)
Untreated
K16ApoE + cp
K16ApoE + dynasore
K16ApoE
B
Clathrin-mediated endocytosis
Counts
FL7 - Int log (AF647)
Untreated
BSA + cp
BSA
BSA + K16ApoE + cp
BSA + K16ApoE
C
BSA uptake at 37 °C
Counts
FL7 - Int log (AF647)
Untreated
BSA
BSA+K16ApoE
D
BSA uptake at 4 °C
Counts
FL7 - Int log (AF647)
Untreated
BSA
BSA+K16ApoE

Figure 3

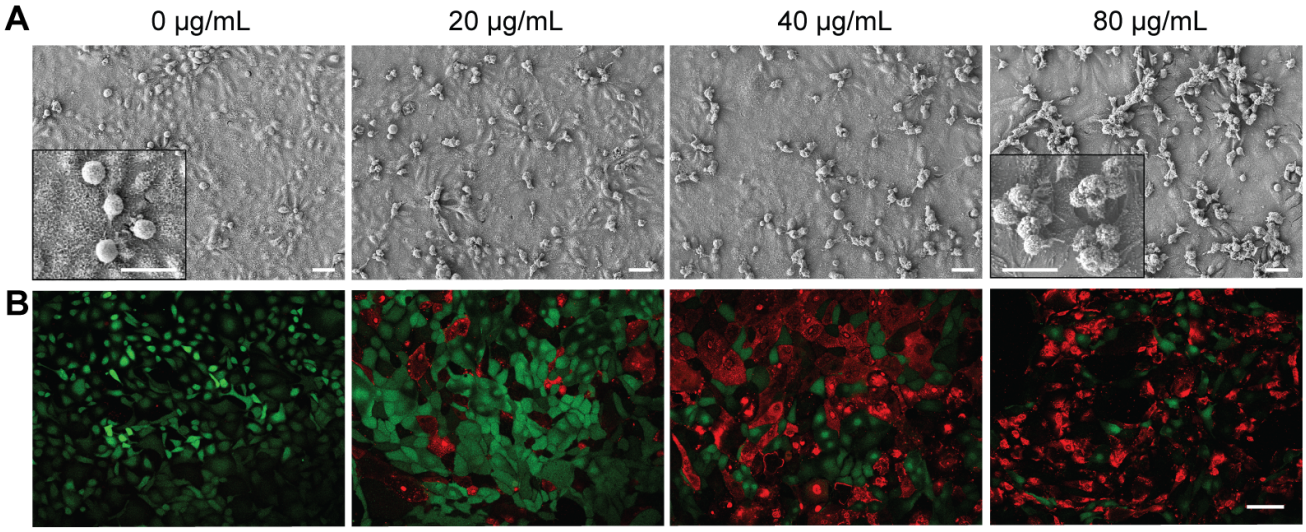
A
0 µg/mL
20 µg/mL
40 µg/mL
80 µg/mL
B

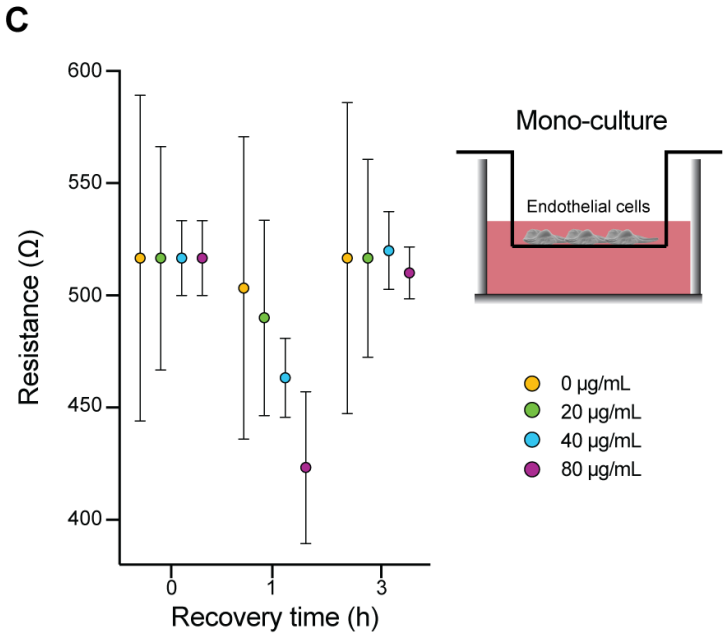
C
600
550
500
450
400
Resistance (Ω)
0
1
3
Recovery time (h)
Mono-culture
Endothelial cells
0 µg/mL
20 µg/mL
40 µg/mL
80 µg/mL

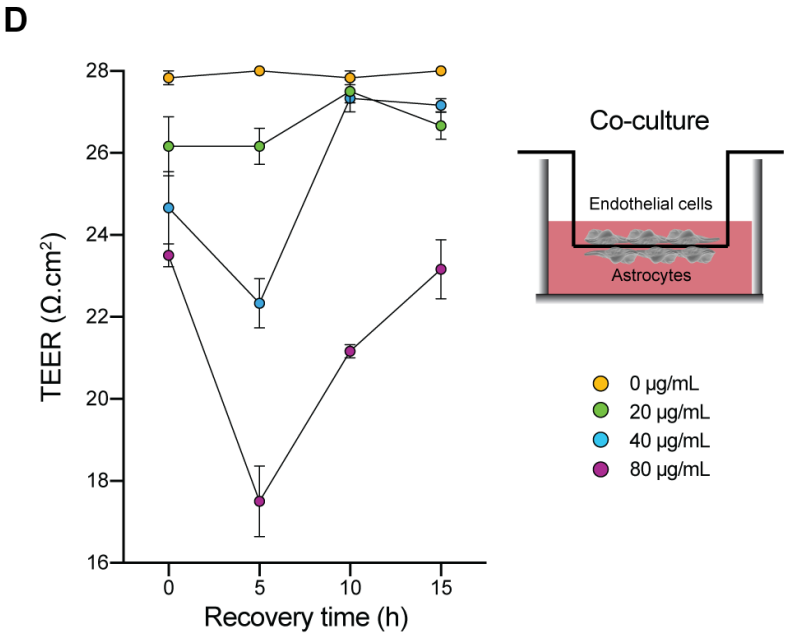
D
28
26
24
22
20
18
16
TEER (Ω.cm²)
0
5
10
15
Recovery time (h)
Co-culture
Endothelial cells
Astrocytes
0 µg/mL
20 µg/mL
40 µg/mL
80 µg/mL

Figure 4

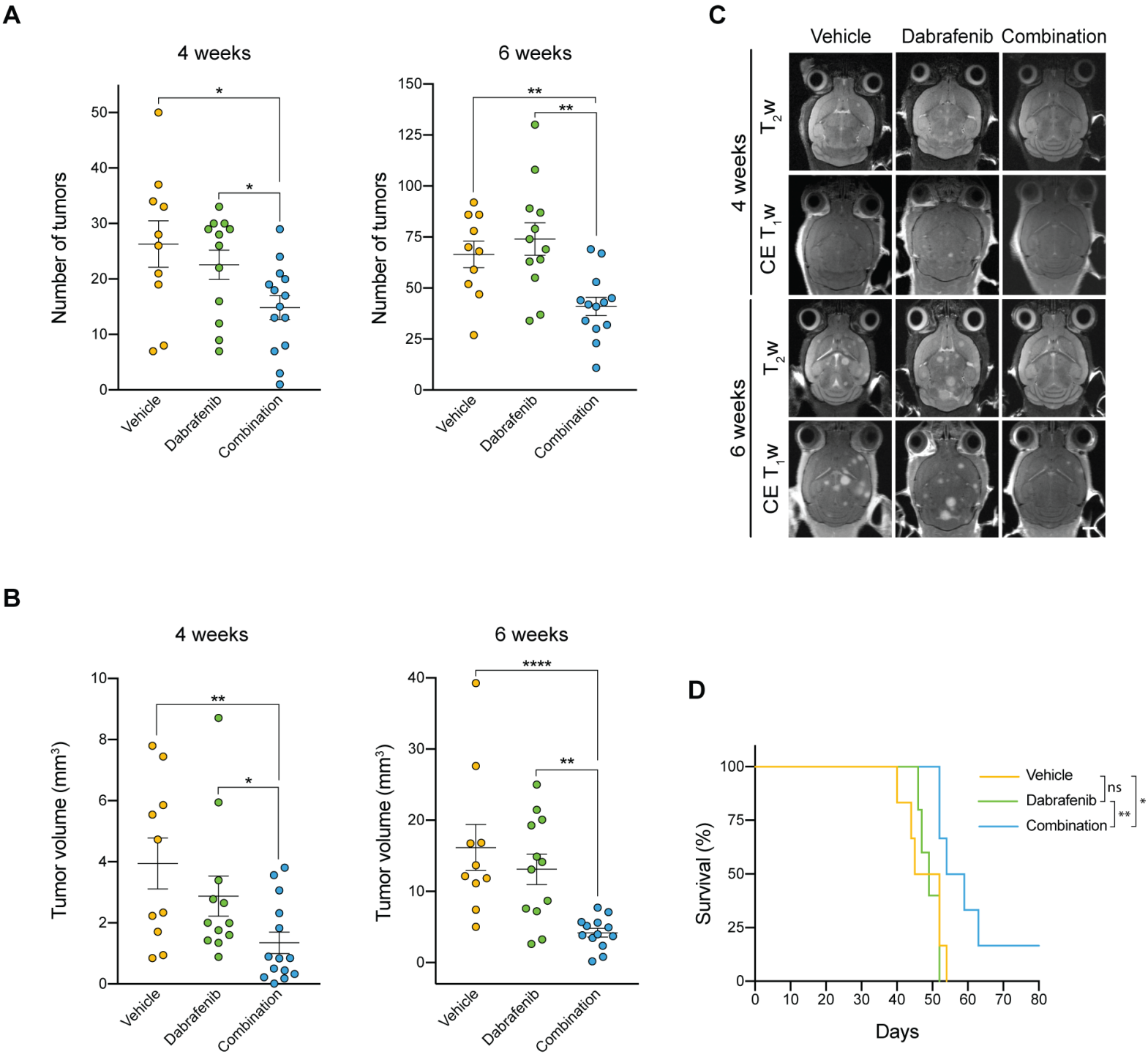
A
4 weeks
6 weeks
Number of tumors
Vehicle
Dabrafenib
Combination
B
Tumor volume (mm³)
C
Vehicle
Dabrafenib
Combination
4 weeks
6 weeks
T2w
CE T1w
D
Survival (%)
Days
ns
*
**
****

Figure 5

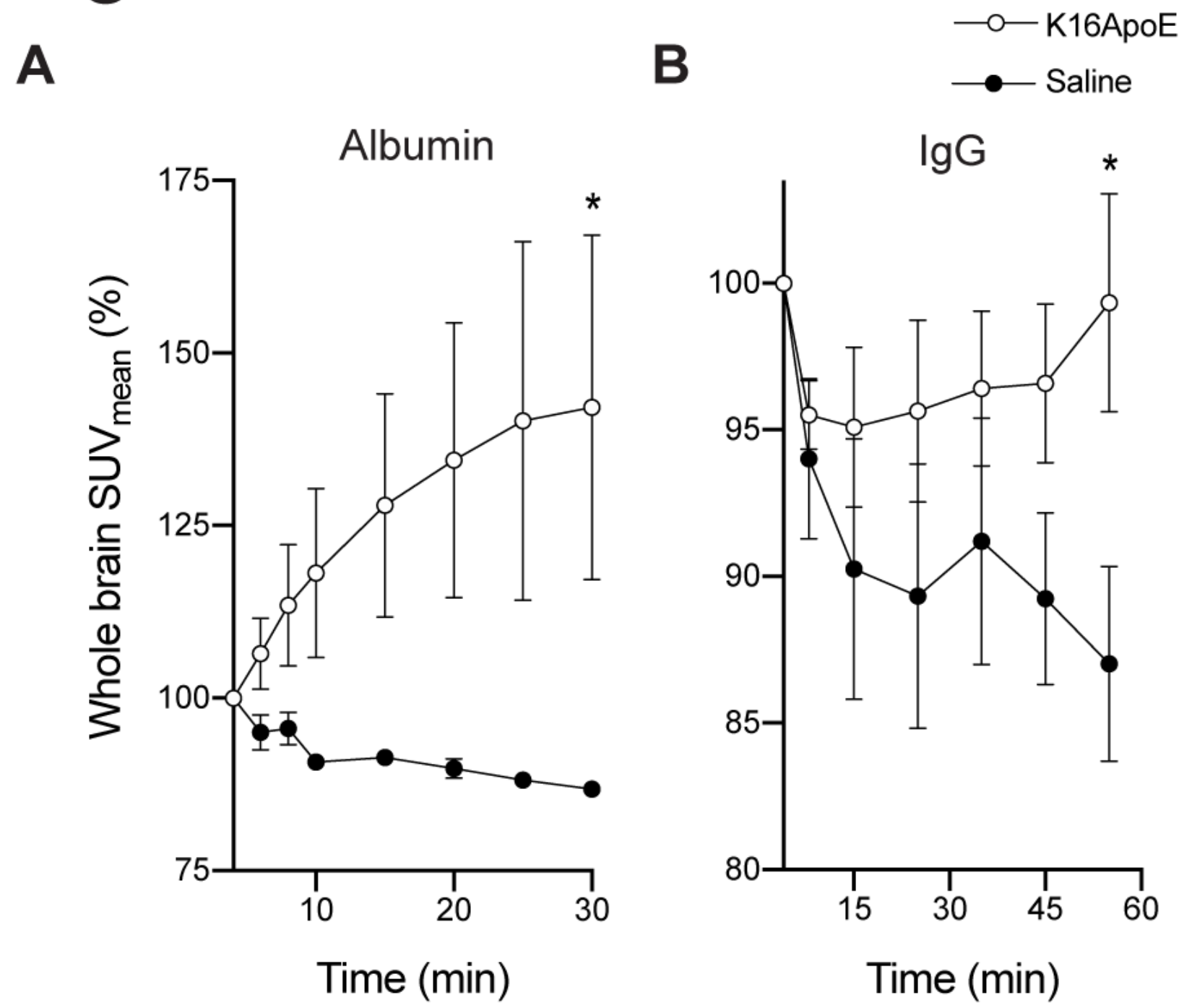
A
Albumin
Whole brain SUV$_{mean}$ (%)
175
150
125
100
75
10
20
30
*
Time (min)
B
K16ApoE
Saline
IgG
100
95
90
85
80
15
30
45
60
*
Time (min)